Understanding subsalt illumination through ray-trace modeling, Part 1: Simple 2-D salt models

DAVID MUERDTER, Diamond Geoscience Research Corporation, Redmond, Washington, U.S.
DAVIS RATCLIFF, Diamond Geophysical Service Corporation, Houston, Texas, U.S.

Coordinated by Guillaume Cambois

The complex structure and high velocity contrast of salt in the Gulf of Mexico create a difficult seismic imaging problem. 3-D prestack depth migration (PreSDM) of seismic data has allowed imaging of reflectors under the salt sheets and of detached bodies of irregular shape. But 3-D PreSDM cannot fill in shadow zones below salt where little energy is reflected. Additionally, amplitude variations caused by salt structures focusing or dispersing seismic energy are usually poorly handled by 3-D PreSDM. Ray-trace modeling can clarify subsalt imaging problems, and the modeling results should be incorporated into exploration and development plans.

The modeling process involves building a computer model that includes salt shapes and velocity variations, simulating an entire 3-D seismic survey with ray-trace modeling, and sorting the data into CRP gathers. Care must be taken in building and ray tracing the model to produce amplitude results that can be compared to seismic amplitudes on subsalt reflectors.

Because of space limitations, this study will appear as a three-part article. This initial paper contains an introduction to ray-trace modeling, ray-trace methods, and examples of simple 2-D salt models. In the second part, more complex models in 2-D and 3-D will be investigated to determine effects of more complicated structures. In the final part, results of ray-traced 3-D models will indicate the effects of shooting direction relative to the structural orientation. In all cases, comparisons are made to similar salt shapes in real seismic data taken from 3-D prestack depth migration surveys in the Gulf of Mexico. This study provides insights into possible imaging anomalies based on simple shapes that can be extrapolated to "real world" situations. However, the complex interplay of real world structure and velocity variations may mean that ray-trace or other modeling is needed to ascertain the specific illumination under these more complex structures.

Advances in seismic technology, particularly 3-D prestack depth migration (PreSDM), were crucial to providing reliable seismic images below salt sheets. These improved seismic images allowed discovery and development of numerous fields in the Gulf of Mexico. Figures 1 and 2 illustrate the difference in imaging and interpretability between 3-D poststack time migration and 3-D prestack depth migration. There remains, however, a need to better understand variations in subsalt imaging quality. For example, high-amplitude anomalies exist under the salt peak in Hickory Field in Grand Island 116 (Figure 2). Are the anomalies caused by a hydrocarbon reservoir, or does focusing of sound energy by the overlying salt peak create these amplitude artifacts?

Seismic modeling can help determine why illumination problems exist, how to interpret them, and what (if any) survey design may better image subsalt horizons. We chose ray-trace modeling for the following reasons:

- Ray-trace results can be sorted into CRP gathers to simulate the effects of 3-D PreSDM.
- Ray-trace plots show visually where sound has traveled, providing an understanding of illumination.
- Ray-tracing produces reasonable approximations of seismic amplitude responses (when care is taken in model making, ray-tracing technique, and ray processing).
- Ray-tracing results can be sorted into common offset bands or common reflection angle bands to understand AVO.
- Ray tracing is a commonly used and proven technology, and commercial software packages are readily available.
- Ray tracing is fast, flexible, and relatively inexpensive compared to full-wave equation modeling.
- Ray tracing, as well as forward modeling in general, can test the effects of variations in selected parameters while keeping the rest of the variables constant.
- These computer simulation results can assess risk factors in using subsalt amplitude anomalies as hydrocarbon indicators.

Ray-trace modeling is commonly used to understand seismic imaging. Sorting rays into CRP gathers has become more common in the last five years, and several ray-trace software packages have been upgraded to contain illumination capabilities.

Approach. This computer ray-trace-modeling study simulates 2-D and 3-D seismic surveys in numerous models, including simple flat models, simple salt shapes, and more complex models, some of which are actual models for parts of the Gulf of Mexico. Simple models isolate a single salt structural element (such as a salt edge or a salt ridge) and determine illumination effects of this element. Real examples of similar structural features are analyzed to determine if effects in the simple model are similar to those in real seismic data from the area. In this way, we hope to build a library of structural features and their responses that can assess other subsalt areas.

In models designed from real examples, known structural and velocity variations were represented in the constructed computer models. The 3-D acquisition geometry used to simulate a 3-D survey followed parameters of actual surveys or simulated possible new parameters, such as shooting in a different direction. Ray-trace

Editor's note: The other two parts of this study—titled "Dipping salt bodies, asymmetry of amplitude response and salt peaks" and "Salt ridges and furrows, shooting orientation of acquisition"—will be published in the July and August issues of TLE.

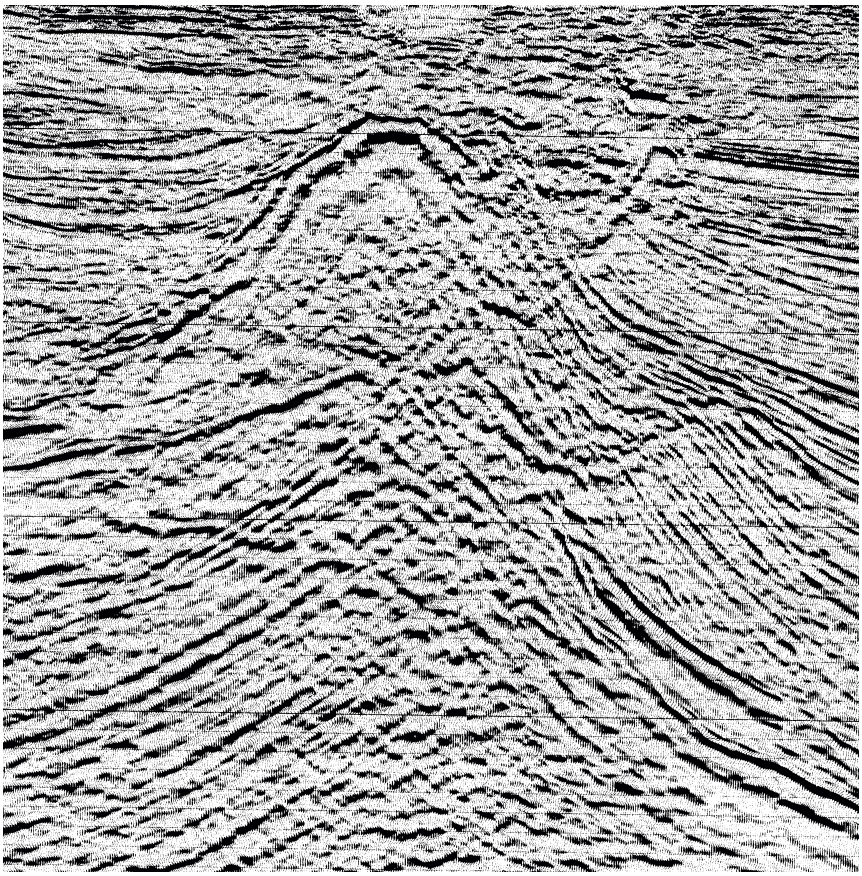

Figure 1. In-line cross-section from Grand Isle South (Hickory) 3-D post-stack time migration.

Table 1. Reasons for variations in seismic amplitude

1. Changes in rock properties below reflecting interface (reservoir rocks) including fluid content, lithology, porosity, and cementation
2. Changes in rock properties of layer overlying the reflector
3. Structure of layers overlying reflector *
4. Velocity field overlying reflector *
5. Dip of reflector *
6. Thickness of the interface (sharp contact or gradational)
7. Changes in thickness between reflector and surrounding interfaces (tuning effects)
8. Acquisition parameters (acquisition footprint)
9. Processing artifacts
10. Viscoelastic properties of overlying rocks including anisotropy and absorption
11. Multiples, noise, mode conversions, etc.

model results are binned into CRP gathers to simulate 3-D PreSDM. Because the reflection coefficient of the reflecting horizon was constant in the model, the amplitude variation maps indicate distortion caused by velocity variations in the overlying structure and by dip of the horizon. Table 1 lists possible reasons for variations in seismic amplitudes.

Models have constant reflection coefficients on subsalt reflecting horizons. Thus lateral changes in rock properties at the reflecting interface did not cause amplitude variations on that horizon. This eliminates items 1 and 2 in Table 1 from the modeling results. In addition, items 6-11 were not modeled because: The modeled reflecting interface is uniformly sharp (item 6); there are no nearby reflectors (item 7); acquisition parameters are constant for the various modeling runs and simulate parameters used in the field (item 8); data are only minimally processed (sorted and t^2 spherical gain correction, item 9); and elastic properties, multiples, noise, and mode conversions were not modeled (items 10-11). Items 3-5 that were modeled are marked with an asterisk (*). Therefore, the resulting reflection-point amplitude maps show the effects of the velocity structure above the reflector and dip of the reflector. One section of this report will vary the acquisition direction to investigate its effect on illumination.

These CRP-gather maps are used in interpretation of the amplitude maps from the existing seismic data. Patterns of amplitude variation in the seismic data that differ from modeled results are due to fluid content of the rock or other reasons. Therefore comparisons of model results with existing 3-D seismic surveys help high-grade drilling targets, such as amplitude anomalies, by providing insight into possible causes for subsalt amplitude variations.

Illumination variations caused by acquisition design can be evaluated by keeping the model constant and only varying acquisition parameters (item 8 in Table 1). Ray tracing two or more survey designs can show variations that different shooting direction or increasing offset length can make to the illumination. The modeling software can model marine cables, bottom cables, vertical cables, and most land layouts. Modeling different designs may help determine if a new survey could improve poorly illuminated areas or if simultaneous processing of two orthogonal surveys would enhance the image.

Angles of reflection of all rays are calculated, and maps of maximum angle of reflection per bin are used to understand the relationship between amplitude variation with angle (AVA) and amplitude variations with offset (AVO). AVO effects can be determined by dividing modeling results into various offset ranges. These offset-limited maps of hits per bin and amplitudes can be valuable in interpreting offset-limited subvolumes generated during processing.

Method. Computer models in this ray-trace study simulate simple structures on the top and base of salt commonly seen in the Gulf of Mexico subsalt trend. Similarly, the velocity field is a generalized version of velocities in the trend. Landmark's DepthTeam (Sierra) software was used to create the models (MIMIC) and for ray-trace simulation (QUIKSHOT). Programs to sort data into CRP bins and to Fresnel-zone smooth the data were created by Diamond Geoscience Research. Some maps were created using Seismic Micro-Technology's 3dPAK, and 3-D visualization was done with Landmark's OpenVision

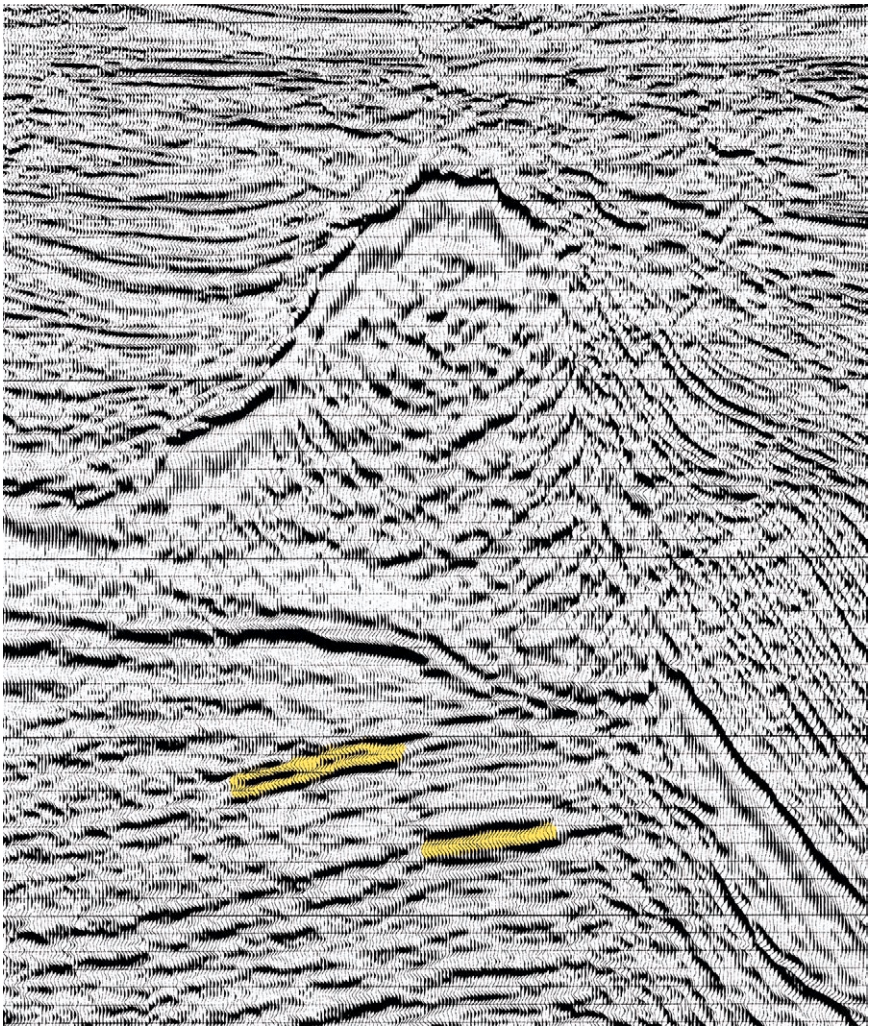

Figure 2. Grand Isle South (Hickory) 3-D prestack depth migration (PreSDM) of same line as in Figure 1. Two high-amplitude anomalies under salt are marked.

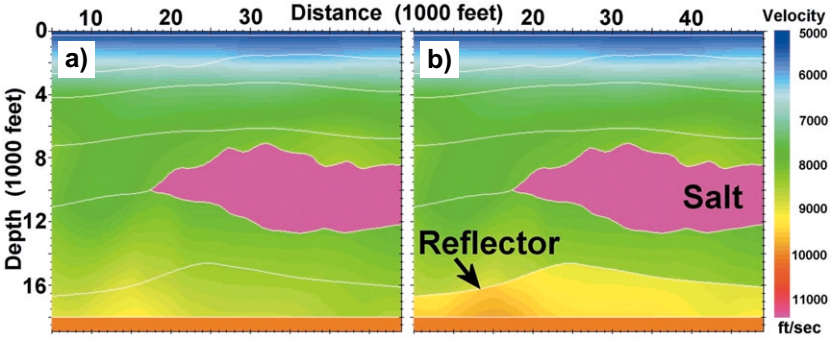

Figure 3. (a) Cross-section through model in Vermilion South area with laterally and vertically varying velocities. (b) Model modified so that reflection horizon has a constant reflection coefficient throughout model. This modification removes changes in the rock property contrast along the horizon as a variable in the modeling.

software. Models ranged from simple 2-D slab models to simple 3-D models of ridges, troughs, peaks, and pits. Salt shapes and velocity fields from real data were used to make 2-D and 3-D models. Ray tracing these more realistic models produced data that can be compared with actual seismic data.

Because ray tracing simulates full-offset acquisition with seismic energy transmitting and reflecting at various angles to the horizons, it is important to model realistic rock properties including density and shear velocity. Realistic amplitude and AVA effects are then calculated. Well logs are used to determine rock properties of the various layers, with Gardner's rule for density and Castagna's relationship for shear velocity used only if no other information is available. In the simple models created to reduce the number of variables and determine the effects of specific structures, the velocities and densities used are simplifications of rock properties in the subsalt trend in the Gulf of Mexico.

To isolate the amplitude variations caused by the overlying salt structure and other velocity variations, models have a constant reflection coefficient over the entire reflecting horizon. A constant reflection coefficient is basic to simple models in which the velocity above and below the reflector does not change laterally. But in a complex model with laterally and vertically varying velocity fields (Figure 3a), care must be taken not to introduce reflection coefficient and AVA variations. In complex models, the model is modified for each horizon ray traced. Rock properties below the horizon are changed (Figure 3b) to create the correct reflection coefficient and AVA for that horizon. Because angle of incidence equals angle of reflection, ray paths to the reflector are unaffected by modification of rock properties below the horizon. But the reflected amplitudes, especially the AVA, are correctly calculated by the modeling software using Zoeppritz's equations.

The complex shapes of salt and the high velocity contrast between salt and the surrounding sediments necessitate a 3-D PreSDM approach to properly image below salt. Likewise, simple "normal incidence" or "image ray" ray-tracing modeling that assumes coincident source and receiver is insufficient for subsalt ray-trace analysis. Our study uses offset ray tracing that simulates actual survey geometries. For 2-D models, all offsets in a single seismic line are simulated (Figure 4a). For a 3-D model, an entire 3-D survey is shot to better represent the complexities of the velocity structure in 3-D.

The various forms of 3-D PreSDM (Kirchhoff, *f-k*, downward continuation) attempt to spatially move sound energy recorded by each receiver for each shot to locations from which they were reflected. Sorting each ray of ray-trace results into reflecting locations or bins is a similar attempt to map energy to its reflection point. The sorted CRP-gather maps produced in the model-

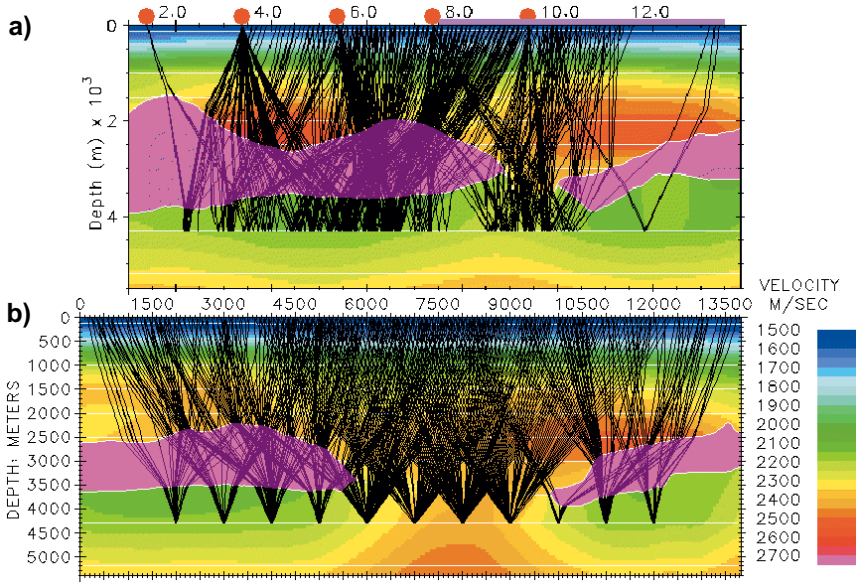

Figure 4. (a) East-west cross-section of Ship Shoal South 3-D model with rays from five shot gathers displayed. The rays reflect from a flat 4300-m subsalt horizon into a 6-km cable (pink horizontal line shows position of cable for a shot at 7500 m along line). For clarity, only every 20th shot is shown (red dot). Note that imaging problems are apparent but are difficult to quantify on this display. (b) Different east-west cross-section from same model showing CRP-gather raypaths for selected bins on a 4300-m subsalt horizon. For clarity, only every 20th CRP is shown. Note that the CRP display is effective in indicating the imaging problems below the salt edge at 10 000 m along the model.

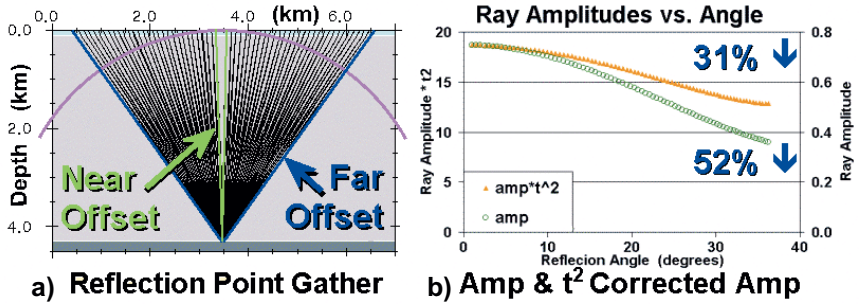

Figure 5. (a) CRP gather in a flat model with a constant velocity field. The pink arc of equal travel distance shows that far-offset rays travel farther and have more spherical spreading. (b) A correction for this extra spherical spreading is needed in the amplitude results, which show a 52% decrease in amplitude in the plot of amplitude versus offset. After a t^2 correction of all the rays, amplitude decreases by only 31% which matches the calculated AVO response of the reflection contrast modeled.

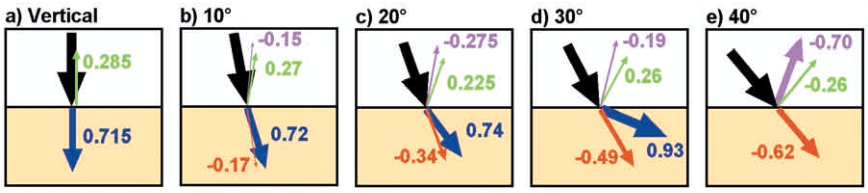

Figure 6. Flat salt interface with division of energy produced by sound impinging at different angles. Rock properties of the overlying sediments are V_P = 2400 m/s, V_S = 896.6, and ρ = 2.167. For the salt V_P = 4450, V_S=2536.5, and ρ = 2.10. Black arrow = impinging *P*-wave energy. Blue = transmitted *P*-wave. Green = reflected *P*-wave. Red = transmitted *S*-wave. Purple = reflected *S*-wave.

ing are plotted to determine shadow areas and areas where seismic energy is concentrated. The visualization of the rays facilitates understanding of subsalt illumination problems (Figure 4b). Ray tracing is computed one horizon at a time, so the imaging results are for a particular horizon, not a volume.

Typical ray-trace shooting parameters were simulated from 50 to 200 m source, receiver, and line spacing and either 6 or 8 km cable lengths. This replicates the geometry of typical Gulf of Mexico surveys but on a sparser grid. Curved rays were simulated except on the simple models where each layer had a constant velocity.

All rays are sorted into CRP gathers. Because the raypath is calculated for each ray, ray-trace results for each horizon can be easily sorted into a grid of bins. An additional step was implemented to spread CRP amplitudes and hits/bin over a Fresnel zone that better represents the interaction of seismic energy with the reflector. Calculations produced the number of hits per bin, total amplitude in the bin, average amplitude for the bin, and minimum, maximum, and average angle of reflections. Because offset is known for each ray, totals can be subdivided into offset ranges. For 3-D ray tracing, maps of these calculated attributes can be made to estimate subsalt illumination.

Because a basic correction in seismic processing is for spherical spreading, all data in this paper are modified with a t^2 correction (amplitude multiplied by the square of two-way traveltime). Therefore modeling results will be more easily compared with actual data. Figure 5 shows a CRP gather in a flat model with constant velocity and the amplitude versus offset plot of the results. In amplitude calculations, the ray-tracing program includes spreading losses. Therefore, there is a 52% decrease in amplitude. After a t^2 correction following ray tracing, amplitude decreases by only 31% which matches the AVO response of the reflector modeled.

With the reflection coefficient and AVA constant for the reflector and with the above corrections, modeled CRP results will reveal amplitude variations related to structural focusing or spreading. Any high amplitudes can be deemed "false" HCIs. Amplitude anomalies from seismic data that match these "false" HCIs should be considered higher risk drilling targets.

Modeling results and observations. Ray tracing simple seismic models is

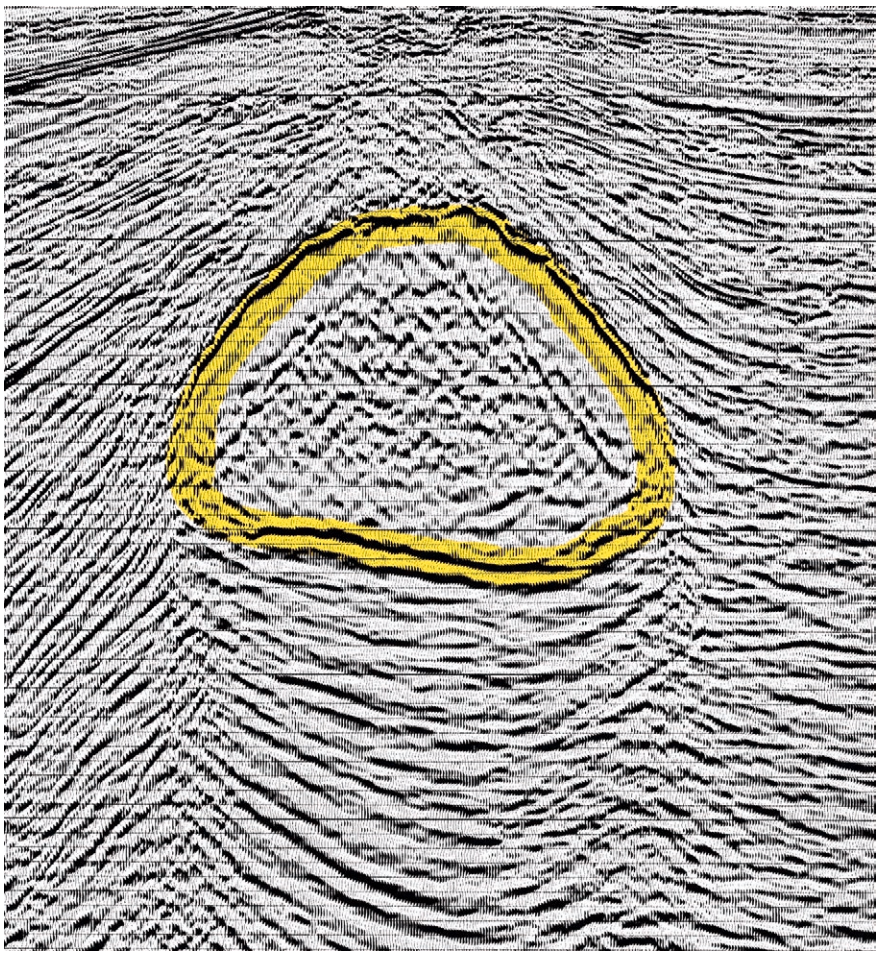

Figure 7. East-west 3-D PreSDM section through salt body in Green Canyon. Note poor imaging and discontinuities under the edges of salt. The top of salt has a dip about 400 on the west and approximately 350 on the east; both are greater than the critical angle for the sediment-salt interface.

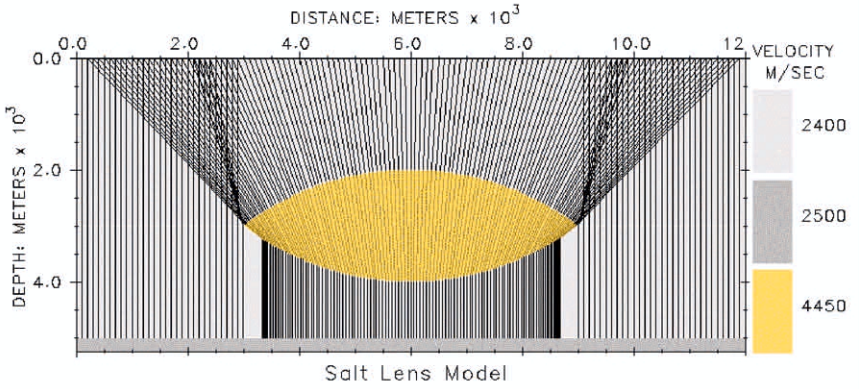

Figure 8. Ray tracing of salt lens model.

an effective way to limit the number of variables and allow manipulation and investigation of each structural and velocity variable. In this study, ray-tracing results from simple models are analyzed to reveal the effects of various salt structures. Analogous examples from the Gulf of Mexico show similar effects in more complex real world models. Observations and conclusions of the modeling results follow each model type to make each section more self-contained and easier to reference.

1) Sediment-salt interface. The simplest model is a single sediment-salt interface (Figure 6) in which low-velocity sediments overlie high-velocity salt. *P*-wave energy impinging on the interface is transmitted and reflected as both compressional and shear waves. For this simple model, the division of energy is directly calculated using the Zoeppritz equations with modeled rock properties and various angles of incidence.

The reflection coefficient at the modeled interface between the 2400 m/s (7874 ft/s) sediments and 4450 m/s (14 600 ft/s) salt is very large, 0.285. With faster sediments of 3000 m/s (9843 ft/s), the reflection coefficient is still large, 0.152. Transmitted energy traveling through salt will be greatly reduced by this partition of energy. Therefore subsalt reflections in which the sound goes down and back up through the salt will be greatly diminished compared to areas without salt.

Figure 6 shows that a vertical *P*-wave ray creates no reflected or transmitted shear-wave rays. As the angle of incidence increases, energy converted to shear becomes more pronounced. Above 32.6° (the critical angle), no transmitted *P*-waves are produced. The nonlinear response of amplitude to angle of incidence is useful and is the basis of AVO theory, but it makes modeling results complex and often nonintuitive.

Normal-incidence ray or image ray modeling assumes that the source and receiver are coincident and that one ray is a valid representation of the response of all stacked rays. This is not valid for subsalt modeling. Therefore in this study, full-offset ray tracing that simulates the entire field array and that models all complexities is used.

Observations from sediment-salt interface response modeling include:

- The large reflections and mode conversions at the sediment-salt interface are important in understanding subsalt imaging. The nonlinear response to sound impinging at various angles on the interface makes subsalt imaging complex and often nonintuitive.
- Full-offset ray tracing is needed to correctly model subsalt illumination.

2) Salt lens. Figure 7 is a seismic section of a lens-shaped salt body from northern Green Canyon in the Gulf of Mexico. Note how the imaging of subsalt reflectors deteriorates near the edge of salt, giving the appearance of discontinuity, possibly a suture zone. Ray tracing of a simple 2-D salt lens model (Figure 8) fashioned after a common double-convex optical lens can produce insights into the imaging discontinuities near edges of salt and

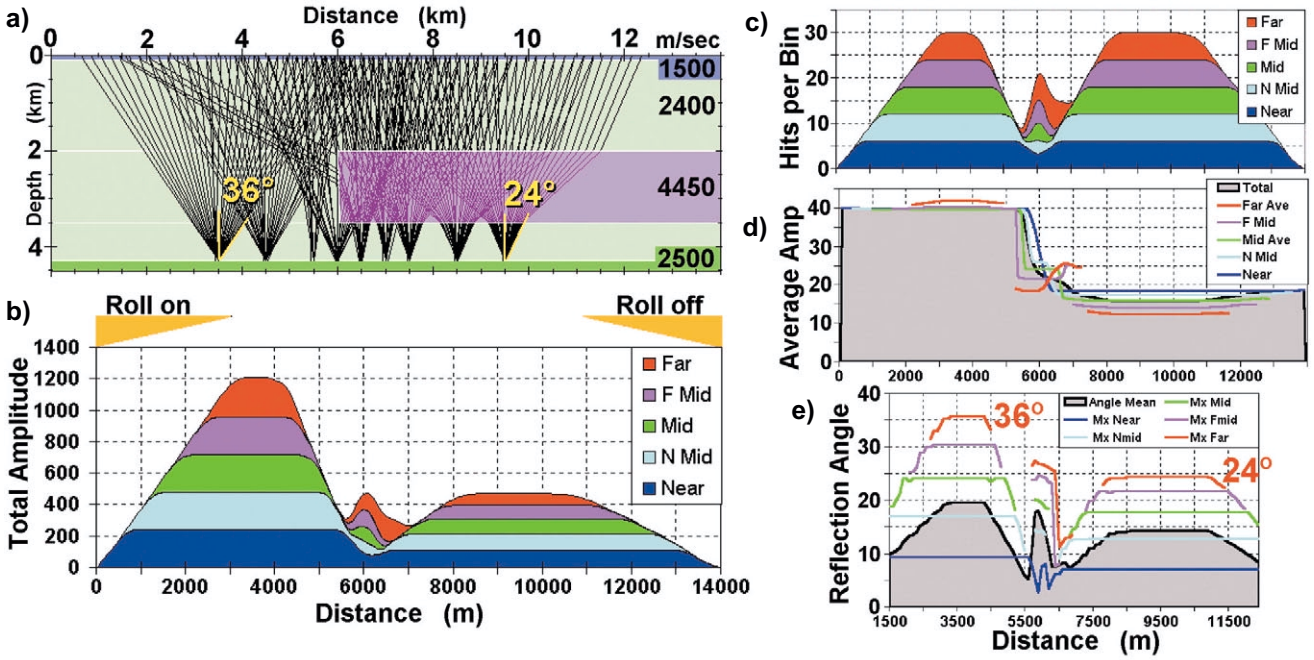

Figure 9. CRP-gather results for near-vertical (89.6° overhang) salt-edge model. (a) Raypaths to selected CRP gathers on model. (b) Total amplitude per bin color-coded by offset range. (c) Hits per bin color-coded by offset range. (d) Average amplitude per bin separated into offset ranges. Note nearly flat AVO signature where there is no salt (all offsets have nearly the same amplitude), but under the salt the amplitude decreases with offset, an effect caused only by the overlying salt. Rock property contrast at the reflector was constant across the model. (e) Maximum angle of reflection for each offset band and the average angle of rays hitting the bins. All data were Fresnel-zone smoothed except for the angle of reflection data.

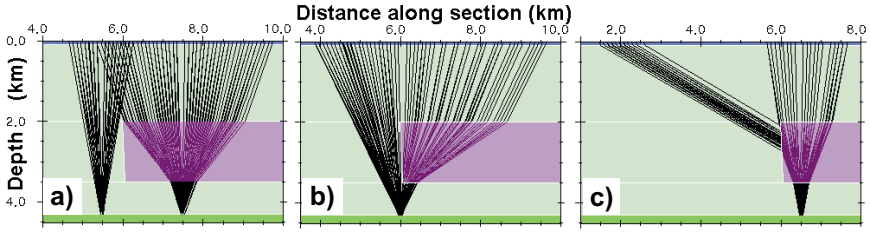

Figure 10. CRP-gather raypaths for selected bins in near-vertical salt edge model. (a) Near-vertical salt face limits far-offset rays in some CRPs. Rays often strike the face beyond critical angle or are refracted away from hydrophones. (b) A small portion of the subsalt reflector is illuminated by rays that travel only once through the salt. (c) Far-offset rays are very sensitive to the exact shape and dip of the salt edge.

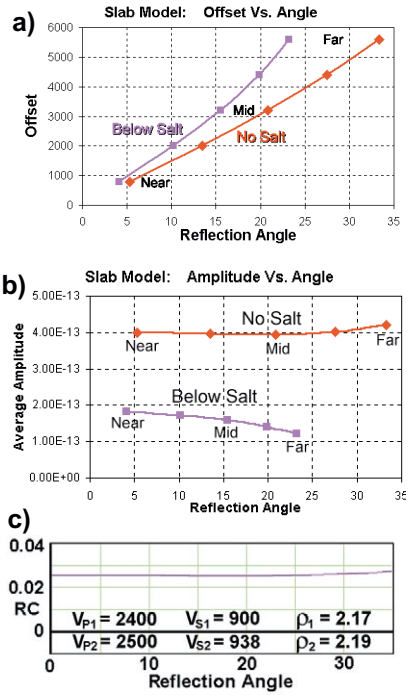

Figure 11. (a) Ray-trace modeling allows calculation of the relation between offset and angle of reflection. (b) AVO effects of the overlying structure and velocity variations can be studied using ray-trace modeling. (c) Theoretical calculations of AVA from rock properties.

can indicate the limits of ray-tracing tools.

To show general imaging effects, the lens model is first ray traced using normal-incidence rays. Normal-incidence rays are perpendicular to the reflector and assume that the source and receiver are coincident (simulating a stacked section). Unlike an optical lens, the salt lens does not focus normal-incidence rays (Figure 8). Sound energy is spread or dispersed because salt has a very high velocity compared to the surrounding Cenozoic sands and shales. We would therefore expect lower amplitudes from subsalt reflections under a lens because of spreading or dispersing of seismic energy.

Another effect seen in both the seismic section (Figure 7) and the salt lens model (Figure 8) is the discontinuity of imaging below the edge of salt. As mentioned in the previous section, normal-incidence ray tracing is too simplified to simulate the complexities of the actual shooting geometry and the AVO effects. Observations from salt lens modeling include:

- Edges of salt bodies produce areas of poor illumination.
- Convex salt bodies tend to disperse sound energy.
- Normal-incidence ray tracing is too simplistic for the complex subsalt

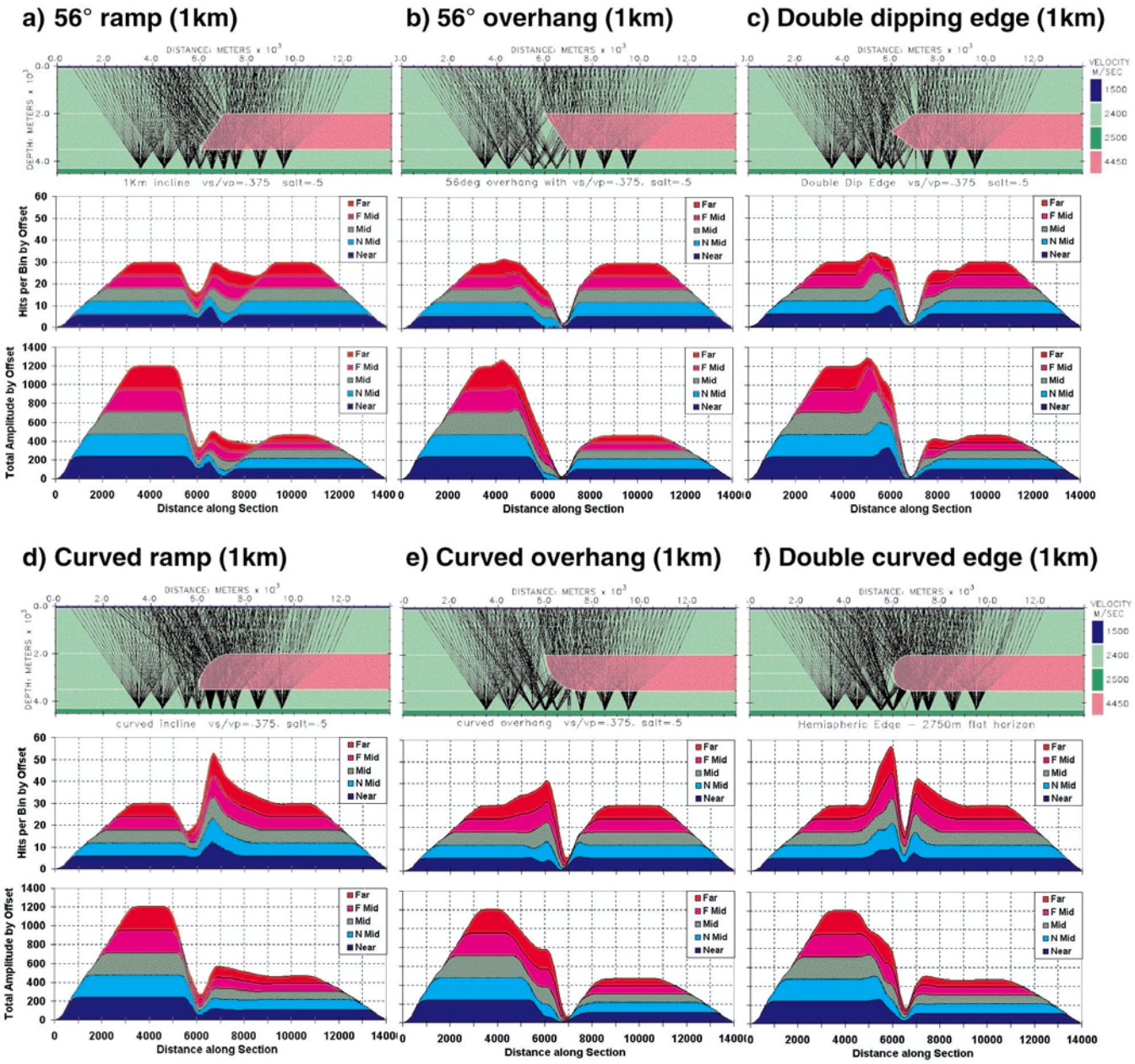

Figure 12. CRP-gather results from salt-edge model. The model with selected CRP raypaths shown above calculated hits/bin and total amplitude plots.

problem. Full-offset ray tracing is needed to correctly model subsalt illumination.

3) Salt-edge models. Simple 2-D models of salt edges were made to investigate imaging effects of variously shaped edges of salt bodies. The models consist of a salt slab with a thickness of 1500 m covering the right half of the model and a deep flat reflector (Figure 9). The salt slab terminates with variously shaped edges in the different models; shapes include salt overhangs and inclined tops of salt that are either linear or with some curvature. These simple models have constant velocities of 1500 ms for a 100 m water layer, 4450 m/s for salt, 2400 m/s for sediments surrounding the salt, and 2500 m/s below the reflector at a depth of 4300 m.

Marine seismic lines were simulated across the models with the following shooting parameters: source and group interval = 100 m; CMP interval = 50 m; maximum offset = 6100 m; and fold = 30. Rays were sorted into 50 m CRP gather bins, and results were separated into offset ranges.

Figure 9 shows illumination results for a near vertical (89.6° overhang) salt-edge model. A maximum offset of 6100 m occurs both outside the salt and under the salt slab away from the salt edge (Figure 9a). Far-offset rays do get through the salt but are sharply refracted and have much smaller maximum angles of reflection—24° under salt compared with 36° where there is no salt. This change can have a significant effect on the AVO response.

The fold chart in Figure 9c shows full fold of 30 hits/bin (rays striking in CRP bin) both outside the salt and under the salt. But the edge of salt has a pronounced effect on the fold. The near vertical salt edge blocks the larger offsets as apparent in individual CMP raypath plots in Figure 10. This effect of the edge starts at less than one half of the maximum offset away from the edge. In different models the distance

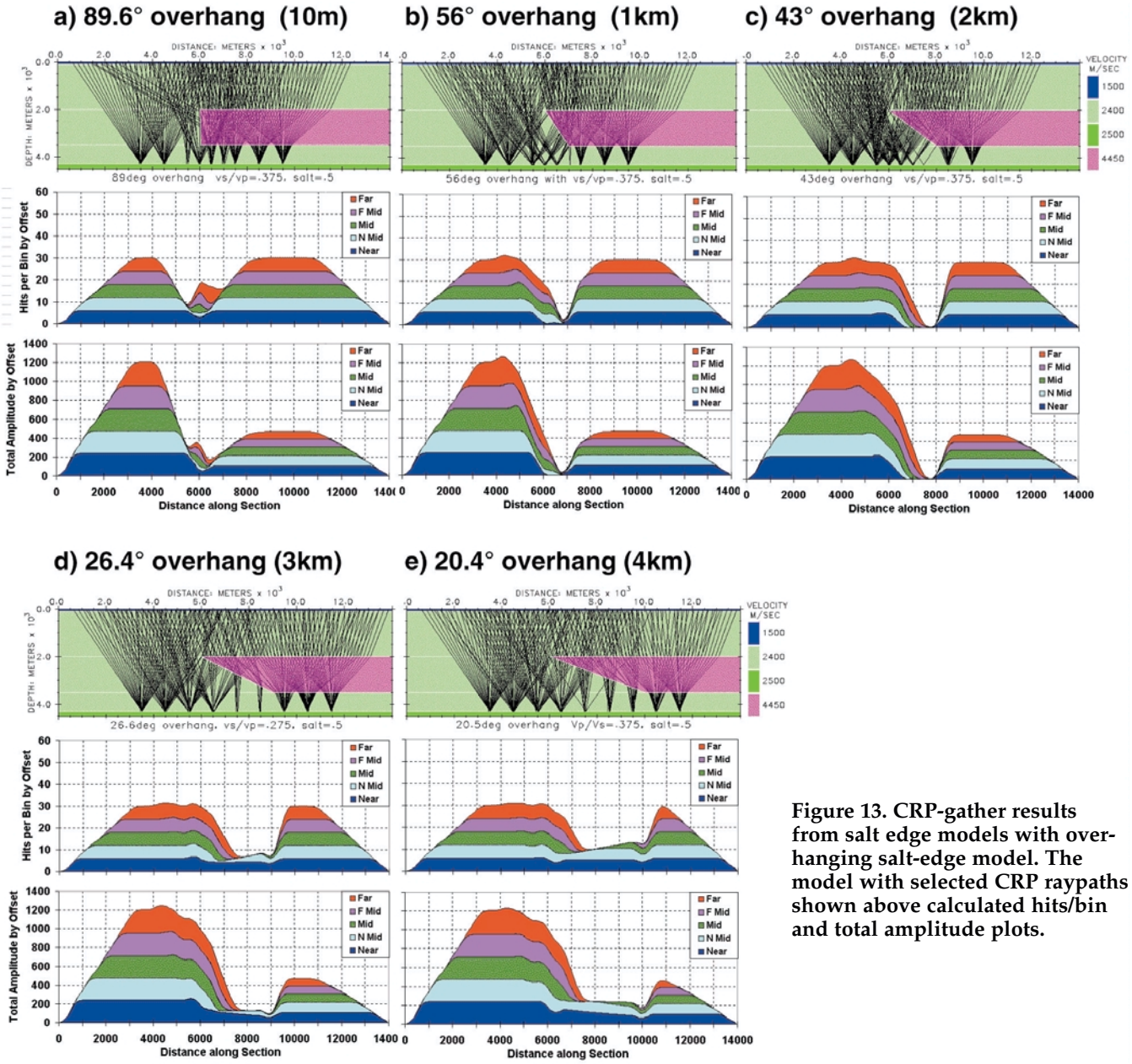

Figure 13. CRP-gather results from salt edge models with overhanging salt-edge model. The model with selected CRP raypaths shown above calculated hits/bin and total amplitude plots.

at which the fold starts to decrease depends on the depth of top salt and the depth of reflector. Fold is increased directly under the salt edge by rays that travel only once through the salt. The slope and shape of the edge determine what rays will pass through the salt edge (Figure 10c). Fold increases from zero to full fold at the left of the section as the array rolls onto the model, and fold decreases at the right because the last source is near the edge of the model.

Total amplitude per bin (Figure 9b) shows a marked decrease under the salt compared to outside the salt. This more than 60% decrease in amplitude is caused by large transmission losses at the four salt-sediment interfaces that the rays pass through, as discussed above. The average or normalized amplitude (total amplitude of all rays in a CRP bin divided by the number of rays, Figure 9d) displays this same reduction in amplitude under salt.

Poor imaging near the edge of salt causes amplitude to greatly diminish, possibly causing the amplitude to be less than the ever-present seismic noise in real data. Seismic processing can fill these reflection "voids" with migration sweeps that give the appearance of discontinuities or salt welds or sutures. The ray-trace modeling used in this study does not simulate diffracted energy that may be present in the shadowed areas under salt edges. Diffractions may be correctly migrated in 3-D PreSDM and provide better illumination than predicted by this study.

The decreased angle of reflection under salt is clear in Figure 9e, which plots the average reflection angle and the maximum angle of incidence for all offset ranges. A plot of offset versus reflection angle (Figure 11a) shows this same effect of reduced angle under the salt. With the angle versus offset relationship known, AVO data can be presented in AVA plots (Figure 11b) that can be directly compared with theoretical rock property AVA calculations (Figure 11c). Note that in this case, the salt causes a change in AVA from slight positive (far offsets have greater amplitude) where no salt exists to a moderate negative AVA under the salt. This effect is due only to the overlying rocks, because the rock property contrast at the reflector is over the entire model.

CRP results for other salt shapes are shown in Figures 12 and 13. All

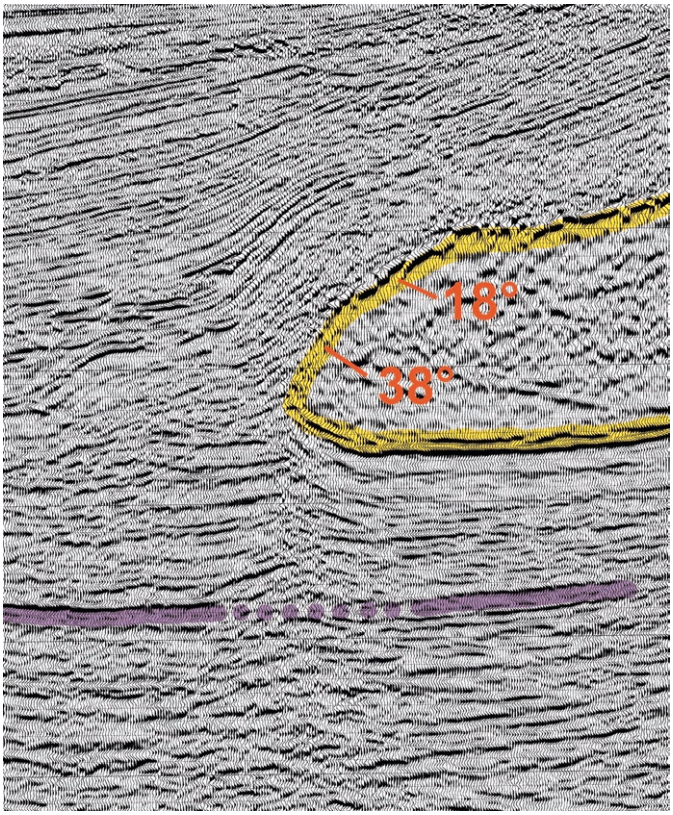

Figure 14. 3-D PreSDM section in north-south orientation (in-line) in the Ship Shoal South area near the Mahogany subsalt field. The salt body outline is yellow. A subsalt reflector is pink. Note the disruption in reflectors below the salt edge. This salt-edge shape is similar to the inclined edge in Figure 12a.

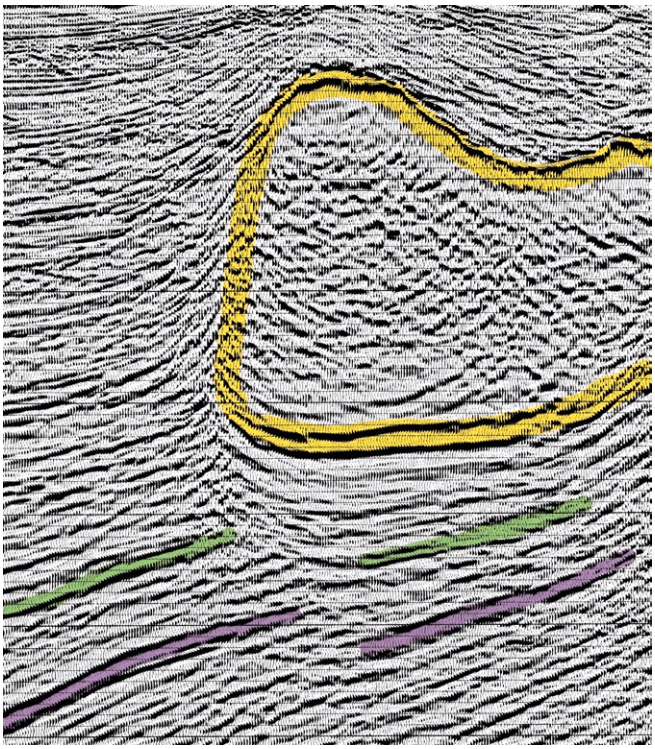

Figure 15. East-west in-line section from a 3-D PreSDM in Garden Banks area. The approximate 80° dip of the salt edge is similar to modeled near-vertical edge in Figure 13a. There is a disturbed zone beneath the salt edge, but subsalt horizons can still be interpreted (colored horizons). There appears to be a fault that is masked by the salt edge disturbance. Imaging is better directly under the edge of salt because reflectors dip away from the salt (see text).

modeled salt edge shapes seriously disrupt imaging under the salt edge. The least disruption occurs where the base of salt is flat and the top of salt is inclined (Figure 12a) even though dip was greater than the critical angle of 32.6°. Overhanging salt edges (Figure 13) cause serious shadowing especially where dip of the overhang is greater than the critical angle (Figures 13b and 13c). When dip is less than the critical angle, near offsets penetrate the salt (Figures 13d and 13e). Observations from salt-edge modeling include:

- Same number of hits per bin (fold) under flat salt slab as in no salt areas
- Maximum angle of reflection reduced under salt
- Reduction of fold under edge of salt. Expect poor signal-to-noise ratio for reflected energy under salt edges. Data processing can fill in these areas of little or no data with migration sweeps.
- Greatly reduced amplitudes under salt (large amplitude loss at each transmission through sediment-salt interface)
- The effect of a salt structure extends as much as half the maximum offset away from the edge of the structure.
- Shape of base of salt edge has greater impact on imaging than shape of the top salt. A combination of top salt dipping in one direction and base dipping in the opposite causes severe disruptions.
- Illuminations are greatly reduced when dip of the top or base of salt approaches or exceeds the critical angle.
- AVO different under salt than outboard of salt because it is affected by transmission through sediment-salt interfaces.

The seismic section in Figure 7 shows great subsalt disturbance under the edges of a salt "pillow." The top of salt near both edges has dip that is greater than the critical angle for the sediment-salt interface. Thus near-offset energy will be blocked and only far-offset energy will illuminate below the salt. A salt suture, if it exists below the edge, is masked by the edge of salt shadow.

In contrast, the relatively gentle salt edge in Figure 14 dips at about 18° for about 1800 m near the edge of salt. The edge is most like the dipping top of salt model in Figure 12a that causes the least amount of subsalt shadowing of the models tested. The area below the 18° area is well imaged and interpretable. In the last 800 m, the salt top steepens to approximately 38°, which is greater than the critical angle. Near offsets are blocked and illumination deteriorates, as shown by the disruption in the reflectors below. But subsalt horizons can be interpreted through the distortion (dotted pink line).

All models shown so far had flat subsalt reflectors. With a flat horizon, reflections are centered above the reflection point. But dipping reflectors, such as those seen in Figure 15, can shift the illumination. The deeper reflectors directly under the steep edge of salt are well imaged because reflections from the near offsets miss the salt body. The salt-edge disturbance shifts under the salt with depth where it partially obscures a fault, if the interpreted correlation is correct. TLE

Corresponding author: D. Muerdter, davem@dgrc.com